Heliyon 7 (2021) e07306

Contents lists available at ScienceDirect

Heliyon

journal homepage: www.cell.com/heliyon

Research article

Wide angle X-ray diffraction patterns and 2D-correlation spectroscopy of crystallization in proton irradiated poly(ether ether ketone)

Abdul G. Al Lafi *, Ali Alzier, Abdul W. Allaf

Department of Chemistry, Atomic Energy Commission, P.O. Box: 6091, Damascus, Syrian Arab Republic

ARTICLE INFO

Keywords:
PEEK
Proton irradiation
2D-CM
X-ray diffraction
Orientation

ABSTRACT

Proton irradiated poly (ether ether ketone) (PEEK) films were crystallized to different extents, and subsequently characterized by wide angle X-ray diffraction technique. The data were analyzed by two-dimensional correlation mapping (2D-CM), in particular: Generalized, hybrid and multiple perturbations correlation approaches. Two asynchronous correlation peaks at (19.1, 18.7) ^{o} and at (22.5, 19.1) ^{o} were utilized as a measure the crystal perfection and the preferred process; orientation/crystal growth respectively. Proton irradiation not only favored the formation of crystal form II, but also changed the type of orientation within the irradiated films. Differential scanning calorimetry and Raman spectroscopic analysis confirmed the contribution of the previous two factors. Raman spectra indicated that the intensity of both bands at 1595 and 1608 cm^{-1} decreased on samples crystallized from the melt, but increased on cold crystallized samples. 2D-CM combined with other suitable techniques is a promising in evaluating the structure of polymers and revealing the effect of proton irradiation.

1. Introduction

Poly (ether ether ketone) (PEEK) is a specialty rather than commodity plastics, having an excellent combination of mechanical strength and material stabilities in severe conditions. These characteristics have motivated the utilization of PEEK in aerospace and nuclear industries [1, 2], besides its application as structural materials for fuel cells, redox flow batteries and high effective adsorbents [3, 4, 5]. The later applications require PEEK to be in the form of highly sulphonated polymer, which elevated the per-cluster volume of SO_3H groups in the membranes, and controls the water uptake, ion exchange capacity (IEC) and consequently proton conductivity of the membranes. Sulphonated PEEK has been produced as blend membranes [6], ternary hybrid membranes having various concentrations of graphene oxide (GO) [7], and as composite membranes [8].

The effects of ion irradiation on PEEK have been the focus of many studies to evaluate the main irradiation mechanism by which the structural, thermal, dielectrical and mechanical properties of PEEK are changed. It has been concluded that crosslinking contributed most to the irradiation chemistry of PEEK [9, 10, 11, 12]. The mechanical characteristics coupled with the expected lifetime of polymers are affected by both crystal type and contents [13]. Wide angle X-ray diffraction (WXRD) is one of the technique that has been successfully adopted to describe crystal type and composition [14, 15]. Moreover, using Rietveld Method [16] to analyze the data leads to structure elucidation and helps to explore the various parameters affecting the structure of materials. However, no evidence related to bond type or new structure formed could be directly reached. Therefore, the combination of WXRD analysis with other analytical tools such as Fourier transformation infra-red (FTIR), and Raman spectroscopies as well as two-dimensional correlation mapping (2D-CM) is necessary [17].

2D-CM, originated by Isao Noda [18], has become an important spectra analysis and interpretation tool in a wide range of spectroscopies [19, 20]. It has been reported to simplify the complex spectra, improve spectral resolution and determine the specific chronological order of spectral intensity variations [18, 20, 21, 22]. 2D-CM techniques have been already applied to analyze X-ray based data including X-ray photoelectron spectroscopy (XPS) [23], particle-induced X-ray emission (PIXE) [24, 25] and small-angle X-ray scattering (SAXS) [26]. Therefore, the major aim of the current study is to investigate the competence of 2D-CM-WXRD to collect evidence related to the nature of the crystal types and structure of proton irradiated PEEK. On the other hand, the results of 2D-CM-WXRD could help to resolve the inconsistency in the literatures about the origin of double melting behavior of PEEK [14, 27, 28, 29] and provide a new insight on the effect of proton irradiation.

* Corresponding author.
E-mail address: cscientific9@aec.org.sy (A.G. Al Lafi).

https://doi.org/10.1016/j.heliyon.2021.e07306
Received 23 July 2020; Received in revised form 28 April 2021; Accepted 9 June 2021

In this paper, WXRD patterns were measured for both cold crystalized and melt crystalized PEEK films after proton irradiation. 2D-CM analysis was applied to evaluate the effect of irradiation on the structure and type of crystals. Differential scanning calorimetry and Raman spectroscopy were used to explain and confirm the 2D-CM findings in relation to type of crystals and orientation within the PEEK films.

2. Experimental

2.1. Materials and proton irradiation

The materials used for this work as well as irradiation facility and conditions have been described in details in previous articles [12, 30].

2.2. FT-Raman spectroscopy

A Thermo Scientific Nicolet 6700 Fourier transform Raman Spectrometer, Madison, USA operating at 1064 nm (Nd: YAG laser) as an exciting frequency, and equipped with an indium gallium-arsenide detector was utilized to analyze PEEK samples. PEEK films were fixed on the suitable accessory and inserted into the 180° scattering geometry compartment. To improve the quality of the spectra, an aluminum foil was used as a carrier for the PEEK films [31]. Spectra were scanned from 100 to 4000 cm^{-1} at 8 cm^{-1} resolution and a total of 200 scans. A separate background spectrum was subtracted after each data acquisition.

2.3. Differential scanning calorimetry (DSC)

The thermal properties of all PEEK samples were measured following the procedure outlined previously for heating/cooling scans as well as for the DSC temperature and enthalpy calibrations [32].

2.4. Wide angle X-ray diffraction (WXRD)

The crystalline structure of all PEEK samples was investigated by the use of a transmission diffractometer (STADI-P STOE, Darmstadt, Germany), with *Cu* K_α radiation ($\lambda = 1.54060\,A$) and a germanium monochromator operated at 50 kV and 30 mA. All WXRD patterns were treated by subtracting a base line (air scatter and amorphous peak) and normalized with respect to the diffraction peak at 20.3°. Finally, all data were arranged in different ways to enable various types of 2D-CM techniques to be utilized.

2.5. 2D correlation analysis

The 2D correlation analysis was carried out following the method developed by Noda [18, 22] and utilizing the 2DShige version 1.3 software (Shigeaki Morita, Kwansei-Gakuin University, 2004–2005**).** A reference patterns (which was taken as the average over all irradiation dose used) was used to correct all patterns intensities. The dynamic patterns were then used to obtain the 2D-CM maps (synchronous and asynchronous) utilizing the discrete Hilbert transform algorithm. In the 2D maps, the red and blue areas reveals positive and negative cross-peaks respectively in both synchronous and asynchronous maps, and they are decoded by Noda's rule [22].

3. Results

3.1. WXRD analysis

Figure 1 shows typical WXRD curves in the region of $2\theta = 10°–36°$ for amorphous, cold crystalized and melt crystalized PEEK. The main reflections peaks are visible at 2θ nearly equal to 19°, 21°, 23° and 29° that are linked with the (110), (111), (200), and (211) planes, respectively [33]. In PEEK, the crystal unit cell has been reported to be

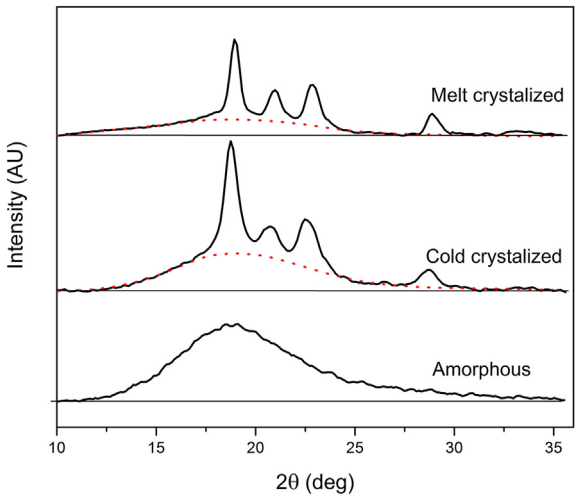

Figure 1. WXRD patterns of amorphous, cold and melt crystallized PEEK.

orthorhombic (space group *Pbcn)* which comprises two chains arranged in a planar zigzag conformation (trans-trans conformation). The crystal unit cell b-axis lines up with the radius of the spherulite, whereas the polymer backbone lines up with the c-axis and is perpendicular to the long dimension of the lamellae and the radius of the spherulite. The crystal unit cell a-axis is perpendicular to the zigzag plane (bc planes). The tilt angle of the phenyl groups relative to the (200) planes is informed to be between 30 and 40° [34]. The preferred growth plane has been shown to be the (110) crystallographic plane, which makes an angle of 52.7° with the radial b-axis [35].

3.2. 2D–COS–WXRD analysis

The following analysis was directed to investigate the alterations of proton irradiation on both the (110) and (200) crystallographic planes, as they provide information about the growth and orientation processes in PEEK respectively.

3.2.1. Crystallization from the melt

All samples were exposed to identical thermal history in the DSC, and after the samples had been crystallized non-isothermally from the melt, their WXRD patterns were collected. The data then were arranged with increasing irradiation dose and analyzed with 2D-CM. The results are presented as synchronous and asynchronous maps in Figure 2 (a) and (b) respectively. The synchronous map, Figure 2(a), shows auto peaks at 2θ equal to 18.7, 19.1, 21.1 and 22.5° and the correlation of 18.7° was the most intense one. Moreover, positive cross-peaks were observed at (21.1, 19.1)° and (22.5, 18.6) ° and negative cross-peaks were observed at (19.1, 18.6) °, (21.1, 18.7) °, (22.5, 19.1) °, (23.1, 18.7) °, (22.5, 21.1) ° and (22.1, 18.7) °. These revealed that the intensity of the reflection peak at 18.7 ° changed in the same direction with that of 22.5 ° but in the contrary direction to the reflection peak at 19.1°.

Figure 2(b) shows the asynchronous map, which reveals the presence of positive cross-peaks that correlated the reflection peaks at (21.1, 18.7) °, (22.5, 19.1) °, (23.1, 18.6) °, (24.5, 18.7) ° and (23.3, 22.5) °. Negative cross-peaks that correlated the reflection peaks at (19.1, 18.6) °, (21.1, 19.1) °, (22.5, 18.7) °, (23.1, 19.1) ° and (23.3, 21.1) ° were also observed. The signs of cross-peaks that deduced from both 2D-CM maps indicated the following sequence of peaks change: 19.1° → 18.6° → 22.5°.

As crystallization occurred from the melt where the chains are freely moved, it is expected that most changes would occur in the preferred growth plane, i.e. (110) represented by the peak at 19.1 °. After the growth to some extent, the crystals oriented with the (200) plane. The low value of the (110) diffraction could be due to the imperfection of

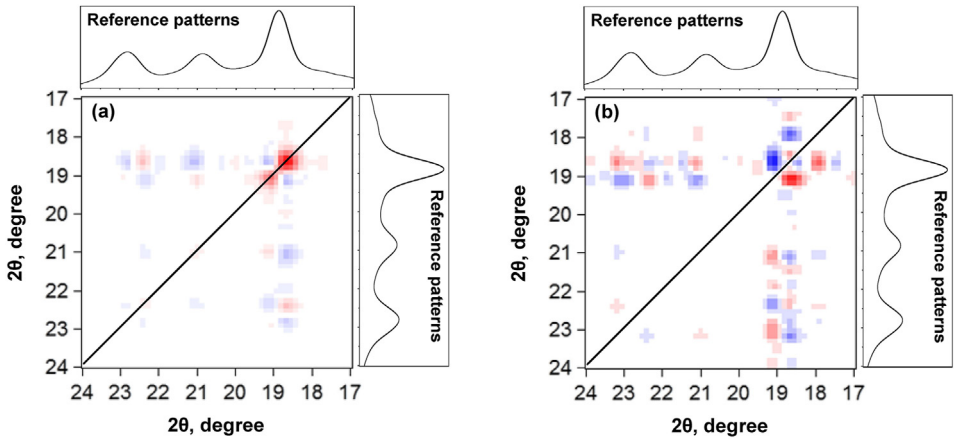

Figure 2. 2D-CM-WXRD maps of melt crystallized proton irradiated PEEK; (a) syncronous and (b) asynchronous.

crystals caused by proton irradiation and the subsequent alteration in the chemical structure of PEEK.

3.2.2. Cold crystallization

All samples were treated at identical conditions in the DSC, and after the samples had been cold crystallized by holding above the glass transition, their WXRD patterns were collected. The data then were arranged with increasing irradiation dose and analyzed with 2D-CM. The results are presented as synchronous and asynchronous maps in Figure 3 (a) and (b) respectively. In the synchronous map, Figure 3(a), there were auto peaks at 2θ equal to 18.7, 19.1 and 23.1° and the correlation of 19.1° was the most intense one. Moreover, positive cross-peaks were observed at (22.4, 18.6) ° and (23.1, 19.1) ° and negative cross-peaks were observed at (19.1, 18.6) °, (21.2, 19.1) °, (22.5, 19.1) °, (23.1, 18.7) ° and (20.6, 19.1) °. The signs of cross-peaks suggested that the intensity of the reflection peak at 18.7° changed in the same direction with that of 22.5° but in the opposite side to the reflection peak at 19.1°.

Figure 3(b) presents the asynchronous map, and shows positive cross-peaks that correlated the reflection peaks at (21.4, 19.1) °, (22.5, 18.6) ° and (23.1, 22.5) °. Negative cross-peaks that correlated the reflection peaks at (19.1, 18.6) °, (21.4, 18.7) °, (22.5, 19.1) °, (23.1, 19.1) ° and (23.1, 21.5) ° were also observed. The signs of cross-peaks from both 2D-CM maps indicated the following series of peaks intensity change: 22.5° → 19.1° → 18.6°.

As crystallization occurred above the glass transition where the movements of chains are restricted, it is expected that most changes would occur in the orientation plane, i.e. the (200) plane represented by the peak at 22.5°. After the chains had taken the suitable orientation, crystals growth started according to the growth plane at 19.1°.

3.2.3. Hybrid 2D-CM approach

The data were accumulated under the same perturbation (irradiation dose) but utilizing different conditions (melt or cold crystallization). To investigate the resemblance and/or discrepancy between the two groups of data, the hybrid 2D approach was used [36, 37].

The results are depicted in Figure 4. Two important correlation peaks were observed, a positive one at (19.1, 18.7) ° and a negative one at (18.4, 18.7) °. The positive peak indicated that the reflection peak at 19.1° in cold crystallized samples changed in the same direction with the reflection peak at 18.7° in melt crystallized samples; both were decreasing. The negative sign of the correlation peak at (18.4, 18.7) ° indicted that the reflection peak at 18.4° was increasing on cold crystallization while the reflection peak at 18.7° was decreasing in melt crystallization. This indicated that more perfect crystals were formed when crystallization occurred from the melt, as the peak shifted to lower values on cold crystallization.

Another positive correlation peak at (19.1, 22.5) ° and a negative one at (22.5, 18.7) ° were observed and confirmed the analysis of generalized 2D-CM, i.e. melt crystallization was governed by growth while cold crystallization was controlled by orientation.

3.2.4. Multiple perturbations 2D-CM approach

In the current work, crystallization was related to both irradiation dose and thermal history. To visualize the dependence on irradiation

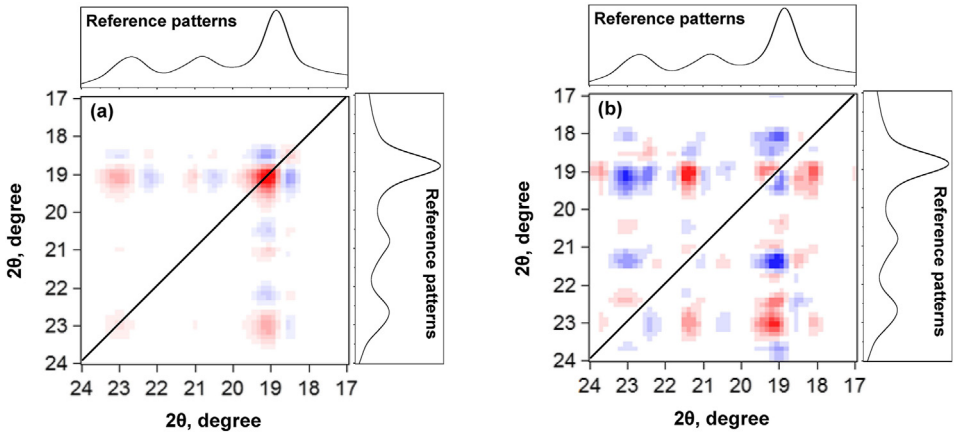

Figure 3. 2D-CM-WXRD maps of cold crystallized proton irradiated PEEK; (a) syncronous and (b) asynchronous.

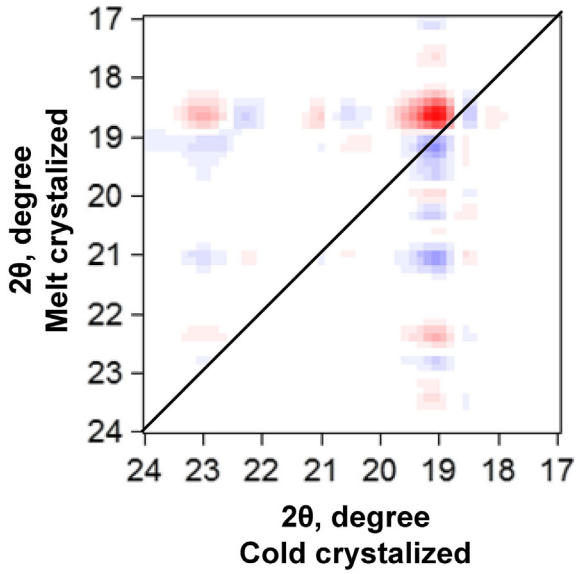

Figure 4. The synchronous 2D-CM-WXRD map of both melt and cold crystallized proton irradiated PEEK. A hybrid approach

dose axe, the approach of multiple perturbation analysis was utilized [38, 39]. The data were reorganized such that each set involved the WXRD patterns of PEEK samples with different thermal history at the same irradiation dose. Each set was analyzed by 2D-CM, and the overall results are presented in Figure 5(a) and (b) as the asynchronous correlation intensity versus the proton irradiation dose.

The two important correlation peaks at (19.1, 18.7) ^{o} and (22.5, 19.1) ^{o} were only considered and discussed. The asynchronous correlation peak at (19.1, 18.7) ^{o} in this case is a measure of the crystal perfection. It was increased with irradiation dose up to 15 MGy and then declined. The increase indicated that irradiation resulted in orientation of the polymer chains, as it has been reported earlier [40], which improved the growth of the crystal. On the other hand, the decrease after 15 MGy, which is above the gelation dose, indicated that the crystal growth had been restricted due the cross-linking and their increasing distribution.

The asynchronous correlation intensity of the cross-peak at (22.5, 19.1) ^{o} on the other hand, is a measure of the preferred process; orientation/thickening or crystal growth. As indicated in Figure 5(b), the intensity of this cross-peak decreased with irradiation dose up to 15 MGy and then increased. The decrease indicated that crystal growth was predominant at lower doses due to the less proportion of units cross-linked and the orientation effect of low irradiation dose. The later increase indicated that crystal growth ceased and orientation become predominant at doses higher than 15 MGy.

4. Discussions

It has been reported that proton irradiated PEEK decomposed thermally in a similar way to that of amorphous PEEK and follows a random chain scission mechanism. PEEK films still have sufficient thermal stability after proton irradiation to the doses used in the present work [30]. Figure 6 was used to confirm the previous fact as well as to confirm that the changes observed in WXRD were due to changes on crystal structure. Moreover, proton irradiation has been reported to introduce marked effects on the DSC behavior of PEEK [41]. The DSC thermograms of amorphous and proton irradiated PEEK samples on first heating scan and on cooling the melt are shown in Figure 6 (a) and (b) respectively. It was

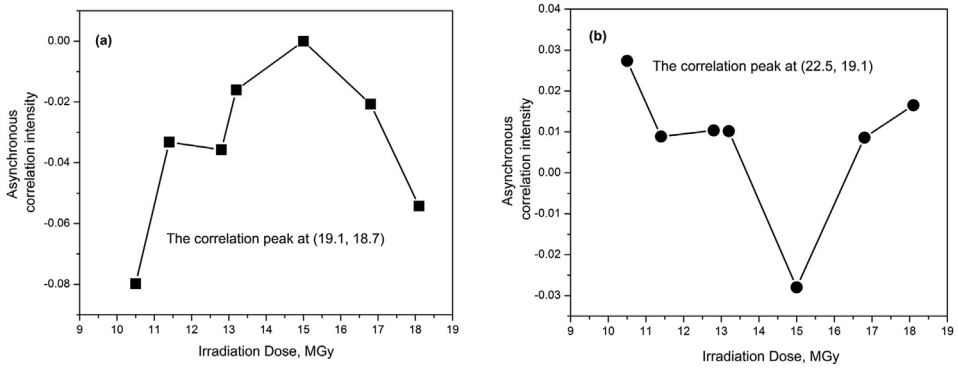

Figure 5. The asynchronous correlation intensities on crystallization of proton irradiated PEEK. (a) The correlation peak at (19.1, 18.7) ^{o} and (b) the correlation peak at (22.5, 19.1) ^{o}.

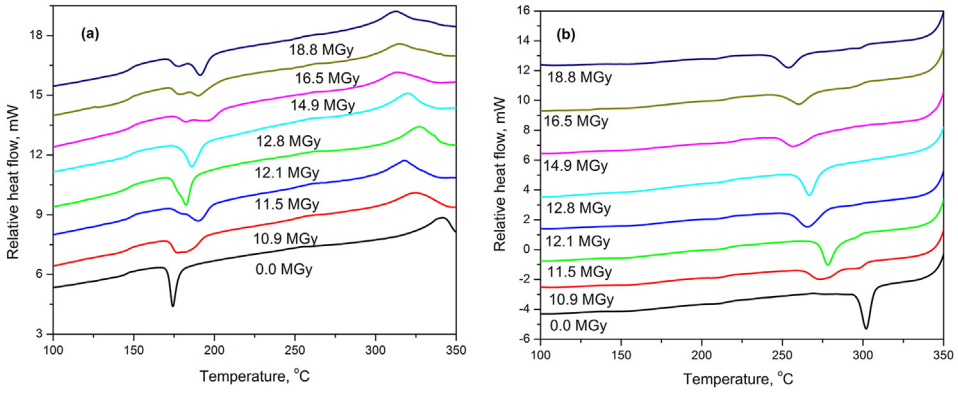

Figure 6. The DSC profiles of amorphous and proton irradiated PEEK films: (a) first heating scan, and (b) cooling scan. Heating/cooling rate was 20 °C min^{-1}.

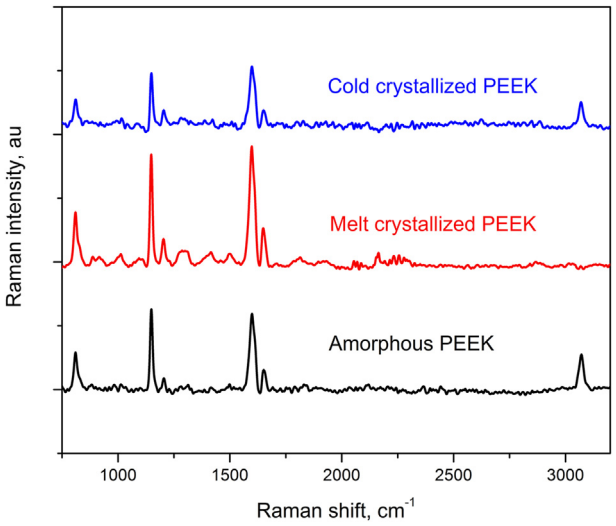

Figure 7. Raman spectra of different crystallinity PEEK samples.

observed that the cold crystallization exothermic peaks split into two components upon proton irradiation. The position of the first one did not appear to change with irradiation dose, while the other one shifted to higher temperatures with increasing irradiation dose. Similar observation was noted in the case of cooling from the melt, and the peak shifted to lower recrystallization temperatures. On the other hand, the endothermic melting peaks appeared to shift to lower temperature with increasing irradiation dose.

As the observed glass transition temperature (Tg) raised with increasing absorbed dose, therefore the restrain on the chain segments increased due to the formation of three-dimensional networks but was incompatible with chain scission [41]. This could account for the shift in cold crystallization and recrystallization temperatures, but could not be used to account for the observed multiple peaks.

Our results indicated that another form of crystals were formed and the driving force was proton irradiation. It has been reported that increasing chain stiffness and decreasing chain mobility, that accompany proton irradiation, made the ability to produce form II significantly enhanced [42]. Liu et al. showed that form II lead to the appearance of a new reflection peak at 16.5°, however, the 2D-CM-WXRD analysis indicated that crystal form II reflection peaks were the same as form I but occurred at lower 2θ values. It has been also reported that irradiation increased the ketone/ether ratio in PEEK and improved chain backing [10, 40]. All these factors enhanced the ability of PEEK to form crystal form II.

Another scenario, which could serve the explanation of the observed changes, could be the change of orientation, as it has been recently reported in the case of block copolymer comprising micro-lamellar and liquid crystal (LC) structures. It has been shown that the periodical lamellar structure initially arranged perpendicular to the fiber axis and rotated by the effect of applied temperature. Eventually, this resulted in the alignment of the periodical lamellar structure parallel to the fiber axis [26].

To understand the influences of proton irradiation on the crystalline structure of PEEK, Raman spectra of all samples were recorded and analyzed. The Raman spectra of amorphous, oriented and crystallized PEEK have been discussed thoroughly in the literature [43]. Typical spectra are shown in Figure 7. The most important spectral features included the carbonyl stretching vibrations, mainly at 1644 cm^{-1}, with a shoulder at 1651 cm^{-1} that has been assigned to disordered and crystalline phases respectively. In addition, in-plane quadrant stretching vibrations of the phenyl rings found at 1608 and 1595 cm^{-1}. It has been reported that the intensity of the two bands at 1595 and 1608 cm^{-1} is

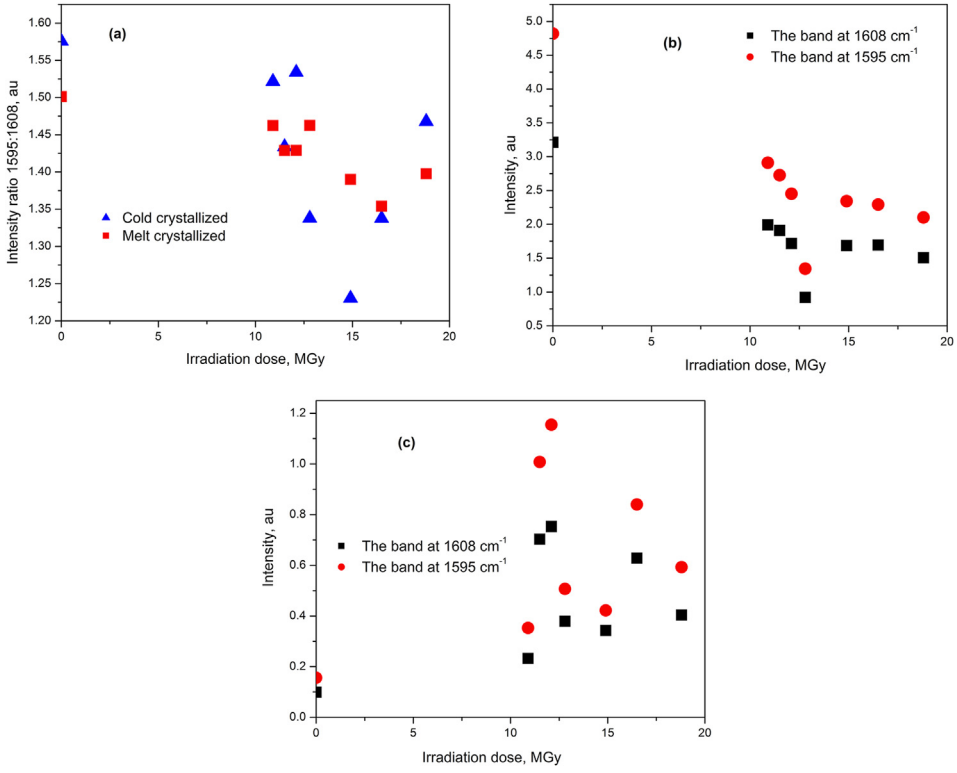

Figure 8. The dependence of 1595 and 1608 cm^{-1} intensities on the irradiation dose of PEEK: (a) The ratio 1595:1608 of both melt and cold crystallized samples, (b) and (c) The intensities of 1595 and 1608 cm^{-1} in melt and cold crystallized samples respectively.

dependent upon both the degree of molecular orientation and the sample position in the laser beam [44].

The intensities of both bands at 1595 and 1608 cm^{-1} were determined by plotting a base line in the region 1680-1550 cm^{-1}, with the help of OMNIC software. The data were plotted in Figure 8 (a), (b) and (c). The ratios 1595:1608 in both cases; melt crystallized or cold crystallized samples were observed to decrease with increasing the irradiation dose, see Figure 8(a). This was attributed to the effect of proton irradiation in decreasing the degree of crystallization, which was in line with both the DSC results and the reported literature [41]. On the other hand, the change in intensity of the two bands at 1595 and 1608 cm^{-1} followed the same trend within the same set of samples; both decreased or increased. It was interesting to note that the intensities of both bands decreased on melt crystallized irradiated samples, see Figure 8(b), but the opposite behavior was observed for the cold crystallized ones, see Figure 8(c).

It has been reported that the direction of intensity change of both bands depend on the orientation, such that the intensities of both bands decreased if the laser beam was perpendicular and they increased if the beam was paralleled [44]. It was concluded that the crystallized chains aligned in different orientation on cold and melt crystallized samples. This was in agreement with the literature [26], and indicated that orientation contributed more than the formation of crystal form II to the observed results. The results were also consistent with the reported FTIR studies of crystallization and proton irradiation effects on PEEK [32, 40]. It has been shown that the relationship between the intensity ratio at 1310/1285 cm^{-1} and crystallization obeyed a linear dependence only when the degree of crystallization was higher than 15% [32]. Both bands were observed to increase in intensity with increasing irradiation dose and were related to molecular chains orientation [40].

As a final remark, the results of the present work were in accordance with the reported literature [45] such that another form of crystal; namely hierarchical spherulitic structure was present in the samples. It seemed that proton irradiation and the cross-linked introduced to the structure of PEEK favored the formation of the second type of crystals.

5. Conclusions

Proton irradiation did not only reduce the final degree of crystallization of PEEK films but also had two further effects: the formation of crystal II type and change the alignment of PEEK chains. With the help of the 2D-CM-WXRD analyses, both effects were observed in the region from $2\theta = 18$ to 24 ^{o} and further indicated that crystal II reflection peaks were the same as form I but occurred at lower 2θ values. The results were confirmed by differential scanning calorimetry analysis, by the splitting of both cold crystallization and melt recrystallization peaks upon proton irradiation. Moreover, Raman spectra indicated that the intensity of both bands at 1595 and 1608 cm^{-1} decreased on samples crystallized from the melt, but increased on cold crystallized samples. It is proposed that proton irradiation improves the mechanical characteristics of PEEK films when irradiation carried to low doses due to the increase in orientation. After the gelation dose (15 MGy), two competing effects, namely the increase in cross-linking and the decrease in crystallinity control the mechanical properties. The combination of specific analytical tools enabled to understand the 2D-CM-WXRD results, and help to envisage the last overview of the influences of proton irradiation in the crystalline structure of PEEK at a molecular level.

Declarations

Author contribution statement

Abdul G. Al Lafi: Conceived and designed the experiments; Analyzed and interpreted the data; Wrote the paper.

Ali Alzier: Performed the experiments.

Abdul W. Allaf: Analyzed and interpreted the data.

Funding statement

This research did not receive any specific grant from funding agencies in the public, commercial, or not-for-profit sectors.

Data availability statement

Data will be made available on request.

Declaration of interests statement

The authors declare no conflict of interest.

Additional information

No additional information is available for this paper.

Acknowledgements

The authors are grateful to Prof. J. N. Hay and Prof. D. J. Parker for their useful comments. The authors are also indebted to Prof. I. Othman the DG of the AEC of Syria for his encouragements.

References

[1] D.J.Y.S. Pagé, H.W. Bonin, V.T. Bui, P.J. Bates, Mixed radiation field effects from a nuclear reactor on poly(aryl ether ether ketone): a melt viscosity study, J. Appl. Polym. Sci. 86 (2002) 2713–2719.

[2] A.M. Díez-Pascual, M. Naffakh, C. Marco, G. Ellis, M.A. Gómez-Fatou, High-performance nanocomposites based on polyetherketones, Prog. Mater. Sci. 57 (2012) 1106–1190.

[3] A.G. Al-Lafi, J.A. Abdullah, R. Hasan, Y. Amin, T. Alnama, Synthesis of cross-linked sulfonated poly(ether ether ketone) and its use for Pb^{2+} and ^{137}Cs removal from aqueous solution, J. Radioanal. Nucl. Chem. 319 (2019) 39–49.

[4] G. Wu, S.-J. Lin, I.-C. Hsu, J.-Y. Su, D.W. Chen, Study of high performance sulfonated polyether ether ketone composite electrolyte membranes, Polymers 11 (2019) 1177.

[5] A.G. Al-Lafi, R. Hasan, N. Al-Kafri, Sulfonated cross-linked poly(ether ether ketone) films with wrinkled structures: preparation and vanadium ions permeability, Macromol. Res. 27 (2019) 1239–1247.

[6] A.R. Kim, M. Vinothkannan, D. JinYoo, Sulfonated-fluorinated copolymer blending membranes containing SPEEK for use as the electrolyte in polymer electrolyte fuel cells (PEFC), Int. J. Hydrogen Energy 42 (2017) 4349–4365.

[7] A.R. Kim, M. Vinothkannan, D. JinYoo, Sulfonated fluorinated multi-block copolymer hybrid containing sulfonated(poly ether ether ketone) and graphene oxide: a ternary hybrid membrane architecture for electrolyte applications in proton exchange membrane fuel cells, J. Energy Chem. 27 (2018) 1247–1260.

[8] A.R. Kim, M. Vinothkannan, M.H. Song, J.-Y. Lee, H.-K. Lee, D. JinYoo, Amine functionalized carbon nanotube (ACNT) filled in sulfonated poly(ether ether ketone) membrane: effects of ACNT in improving polymer electrolyte fuel cell performance under reduced relative humidity, Compos. B Eng. 188 (2020) 107890.

[9] T. Sasuga, H. Kudoh, Ion irradiation effects on thermal and mechanical properties of poly (ether-ether-ketone) PEEK, Polymer 41 (2000) 185–194.

[10] A.G. Al-Lafi, Structural development in ion-irradiated poly(ether ether ketone) as studied by dielectric relaxation spectroscopy, J. Appl. Polym. Sci. 131 (2014) 2593–2601.

[11] A. Mackova`, V. Havranek, V. Svorcik, N. Djourelov, T. Suzuki, Degradation of PET, PEEK and PI induced by irradiation with 150 keV Ar^{+} and 1.76 MeV He^{+} ions, Nucl. Instrum. Methods Phys. Res. B 240 (2005) 245–249.

[12] A.G. Al-Lafi, The effects of ion irradiation on the dielectric properties of poly(ether ether ketone), Polym. Bull. 68 (2012) 2269–2283.

[13] D.J.T. Hill, D.A. Lewis, J.H. O'Donnell, A.K. Whittaker, The crosslinking mechanism in gamma irradiation of polyarylsulfone: evidence for Y-links, Polym. Adv. Technol. 9 (1998) 45–51.

[14] M.J. Jenkins, J.N. Hay, N.J. Terrill, Structure evolution in melt crystallized PEEK, Polymer 44 (2003) 6781–6787.

[15] D.J. Blundell, V. Bayon, The crystal structure of poly(ether ketone) copolymers, Polymer 34 (1993) 1354–1360.

[16] B.H. Toby, EXPGUI, a graphical user interface for GSAS, J. Appl. Crystallogr. 34 (2001) 210–213.

[17] A.G. Al-Lafi, B. Assfour, T. Assaad, Metal organic framework MIL-101(Cr): spectroscopic investigations to reveal Iodine capture mechanism, J. Inorg. Organomet. Polym. Mater. 30 (2020) 1218–1230.

[18] I. Noda, Generalized two-dimensional correlation method applicable to infrared, Raman, and other types of spectroscopy, Appl. Spectrosc. 47 (1993) 1329–1336. http://www.opticsinfobase.org/as/abstract.cfm?URI=as-47-9-1329.

[19] I. Noda, Close-up view on the inner workings of two-dimensional correlation spectroscopy, Vib. Spectrosc. 60 (2012) 146–153.

[20] Y. Park, S. Jin, I. Noda, Y.M. Jung, Recent progresses in two-dimensional correlation spectroscopy (2D-COS), J. Mol. Struct. 1168 (2018).
[21] I. Noda, Progress in two-dimensional (2D) correlation spectroscopy, J. Mol. Struct. 799 (2006) 2–15.
[22] I. Noda, Y. Ozaki, Two-Dimensional Correlation Spectroscopy:Applications in Vibrational and Optical Spectroscopy, Wiley, Chichester, 2004.
[23] A.G. Al-Lafi, Application of 2D correlation methods to the analysis of XPS spectra of ion irradiated poly (ether ether ketone), J. Polym. Res. 25 (2018) 105.
[24] A.G. Al-Lafi, M.S. Rihawy, PIXE data analysis by two-dimensional correlation mapping techniques: analysis of chloride and sulfate ions attack in homemade mortar samples, X Ray Spectrom. 49 (2020) 379–389.
[25] A.G. Al-Lafi, M.S. Rihawy, RBS and PIXE data analysis by two dimensional correlation mapping techniques: on the effects of ion irradiation and sulfonation on poly(ether ether ketone) membranes, X Ray Spectrom. 50 (2021) 121–133.
[26] M. Koga, M. Tokita, J. Mizukadoa, H. Shinzawa, Two-dimensional (2D) small-angle X-ray scattering (SAXS) correlation spectroscopy for block copolymer consisting of microlamellar and liquid crystal (LC) structures, J. Mol. Struct. 1207 (2020) 127767.
[27] C.-L. Wei, M. Chen, F.-E. Yu, Temperature modulated DSC and DSC studies on the origin of double melting peaks in poly(ether ether ketone), Polymer 44 (2003) 8185–8193.
[28] H. Marand, A. Alizadeh, R. Farmer, R. Desai, V. Velikov, Influence of structural and topological constraints on the crystallization and melting behavior of polymers. 2. Poly(arylene ether ether ketone), Macromolecules 33 (2000) 3392–3403.
[29] D.A. Ivanov, R. Legras, A.M. Jonas, Interdependencies between the evolution of amorphous and crystalline regions during isothermal cold crystallization of poly(ether-ether-ketone), Macromolecules 32 (1999) 1582–1592.
[30] A.G. Al-Lafi, J.N. Hay, D.J. Parker, The effect of ion irradiation on the thermal properties of poly(ether ether ketone), J. Polym. Sci. B Polym. Phys. 46 (2008) 2212–2221.
[31] L. Cui, H.J. Butler, P.L. Martin-Hirsch, F.L. Martin, Aluminium foil as a potential substrate for ATR-FTIR, transflection FTIR or Raman spectrochemical analysis of biological specimens, Anal. Meth. 8 (2016) 481–487.
[32] A.G. Al-Lafi, A. Alzier, A.W. Allaf, Two-dimensional FTIR spectroscopic analysis of crystallization in cross-linked poly(ether ether ketone), Int. J. Plast. Technol. 24 (2020).
[33] J.N. Hay, J.I. Langford, J.R. Lloyd, Variation in unit cell parameters of aromatic polymers with crystallization temperature, Polymer 30 (1989) 489–493.
[34] O. Dupont, A.M. Jonas, R. Legras, Adaptation of the Rietveld method for the characterization of the lamellar microstructure of polymers, J. Appl. Crystallogr. 30 (1997) 921–931.
[35] S. Kumar, D.P. Anderson, W.W. Adams, Crystallization and morphology of poly(aryl-ether-ether-ketone), Polymer 27 (1986) 329–336.
[36] Y. Wu, J.-H. Jiang, Y. Ozaki, A new possibility of generalized two-dimensional correlation spectroscopy: hybrid two-dimensional correlation spectroscopy, J. Phys. Chem. 106 (2002) 2422–2429.
[37] Y. Wu, F. Meersman, Y. Ozaki, A novel application of hybrid two-dimensional correlation infrared spectroscopy: exploration of the reversibility of the pressure- and temperature-induced phase separation of poly(N-isopropylacrylamide) and poly(N-isopropylmethacrylamide) in aqueous solution, Macromolecules 39 (2006) 1182–1188.
[38] H. Shinzawa, K. Awa, I. Noda, Y. Ozaki, Multiple-perturbation two-dimensional near-infrared correlation study of time-dependent water absorption behavior of cellulose affected by pressure, Appl. Spectrosc. 67 (2013) 163–170.
[39] A.G. Al-Lafi, J.N. Hay, State of the water in crosslinked sulfonated poly(ether ether ketone). Two-dimensional differential scanning calorimetry correlation mapping, Thermochim. Acta 612 (2015) 63–69.
[40] A.G. Al-Lafi, FTIR spectroscopic analysis of ion irradiated poly (ether ether ketone), Polym. Degrad. Stabil. 105 (2014) 122–133.
[41] A.G. Al-Lafi, J.N. Hay, D.J. Parker, The effect of proton irradiation on the melting and isothermal crystallization of poly(ether ether ketone), J. Polym. Sci. B Polym. Phys. 46 (2008) 1094–1113.
[42] T. Liu, S. Wang, Z. Mo, H. Zhang, Crystal structure and drawing-induced polymorphism in poly(aryl ether ether ketone). IV, J. Appl. Polym. Sci. 73 (1999) 237–243.
[43] G. Ellis, M. Naffakh, C. Marco, P.J. Hendra, Fourier transform Raman spectroscopy in the study of technological polymers Part 1: poly(aryl ether ketones), their composites and blends, Spectrochim. Acta 53 (1997) 2279–2294.
[44] N.J. Everall, J. Lumsdon, J.M. Chalmers, N. Mason, The use of polarised Fourier transform Raman spectroscopy in morphological studies of uniaxially oriented PEEK fibres—some preliminary results, Spectrochim. Acta 47 (1991) 1305–1311.
[45] Y. Wang, J.D. Beard, K.E. Evans, O. Ghita, Unusual crystalline morphology of poly aryl ether ketones (PAEKs), RSC Adv. 6 (2016) 3198–3209.